Materiales de Construcción 75 (360)
October-December 2025, e390
ISSN-L: 0465-2746, eISSN: 1988-3226
https://doi.org/10.3989/mc.2025.395224

Mineral formation process and environmental benefits of belite-ye'elimite cement clinker from industrial solid wastes

C. Sun [a], C. Yan [b,c,d] ✉, J. Zhang [c,d,e,] ✉, R. Bai [f], L. Jing [b], T. Bold[g]

a. College of science, Inner Mongolia University of Technology, (Hohhot, China)
b. College of resources and environmental engineering, Inner Mongolia University of Technology, (Hohhot, China)
c. Inner Mongolia Autonomous Region Engineering Research Center for Eco-Building Materials and Fabricated Structure, (Hohhot, China)
d. The Key Lab. of Green Development for Mineral Resources, Inner Mongolia University of Technology, (Hohhot, China)
e. School of Civil Engineering, Inner Mongolia University of Technology, (Hohhot, China)
f. School of materials science and engineering, Inner Mongolia University of Technology, (Hohhot, China)
g. School of applied sciences, Mongolian University of science and Technology, (Ulaanbaatar, Mongolia)
✉: ycw20031013@126.com
✉: zj970741@imut.edu.cn

Received 10 September 2024
Accepted 18 June 2025
Available on line 13 January 2026

ABSTRACT: To optimize resource utilization of bulk industrial solid waste and promote low-carbon production in the cement industry, the belite-ye'elimite cement (BSAC) clinker was prepared entirely from solid waste materials (carbide ash, coal gangue, steel slag, desulfurization gypsum). The mineral formation process of the clinker was systematically analyzed. Findings reveal that within the temperature range of 700-1100 ºC, the clinker primarily comprises transition minerals such as aluminosilicate, aluminate, calcium sulphosilicate. At 1100-1200 ºC, these phases gradually convert to dicalcium silicate (C_2S) and ye'elimite ($C_4A_3\check{S}$). Above 1200 ºC, changes in the minerals correlate to the structural and morphological evolution of C_2S and $C_4A_3\check{S}$ crystals. However, beyond 1320 ºC, C_2S exhibit an irregular morphology, and $C_4A_3\check{S}$ decomposes. BSAC prepared at 1260 °C met the mechanical requirements for 52.5 grade sulphoaluminate cement. Environmentally, BSAC clinker reduces energy consumption by 18% and carbon emissions by 65% compared to traditional Portland cement.

KEY WORDS: Solid waste; Cement clinker; Mineral formation; Environmental assessment.

Citation/Citar como: Sun C, Yan CW, Zhang J, Bai R, Jing L, Boldg T. 2025. Mineral formation process and environmental benefits of belite-ye'elimite cement clinker from industrial solid wastes. Mater. Construcc. 75(360):e390. https://doi.org/10.3989/mc.2025.395224

RESUMEN: *Proceso de formación mineral y beneficios ambientales del clínker de cemento belita-ye'elimita a partir de residuos sólidos industriales***.** Para optimizar el aprovechamiento de residuos sólidos industriales masivos y promover la producción baja en carbono en la industria cementera, se preparó un clínquer de cemento belita-ye'elimita (BSAC) exclusivamente con materiales residuales (ceniza de carburo, ganga carbonosa, escoria siderúrgica, yeso de desulfuración). Se analizó sistemáticamente el proceso de formación mineral del clínquer. Los resultados demuestran que dentro del rango de 700-1100 °C predominan minerales transitorios como aluminosilicatos, aluminatos y sulfoaluminatos cálcicos. Entre 1100-1200 °C, estas fases se transforman gradualmente en silicato dicálcico (C_2S) y ye'elimita ($C_4A_3\check{S}$). Por encima de 1200 °C, los cambios minerales se correlacionan con la evolución estructural y morfológica de los cristales de C_2S y $C_4A_3\check{S}$. Sin embargo, al superar 1320 °C, el C_2S presenta morfología irregular y el $C_4A_3\check{S}$ se descompone. El BSAC sintetizado a 1260 °C cumple los requisitos mecánicos del cemento sulfoaluminoso grado 52.5, reduciendo un 18% el consumo energético y un 65% las emisiones de carbono comparado con el cemento Portland tradicional.

PALABRAS CLAVE: Residuos sólidos; Clínker de cemento; Formación mineral; Evaluación ambiental.

1. INTRODUCTION

Silicate cement, a primary building material, is consumed extensively in China (1). According to statistics, China's cement production reached 2.02 billion tons in 2023, the highest globally (2). However, cement manufacturing is classified as a high-consumption, high-pollution industry (3, 4). The production of one ton of silicate cement clinker requires 1324 kg of limestone, 238 kg of clay, 113 kg of coal, and 128 kWh of electrical energy, while emitting approximately 920 kg of CO_2 (5). This high-pollution and high-energy consumption production model runs counter to the goals of sustainable development.

Within this context, belite-ye'elimite cement, a novel type of sulfoaluminate cement, demonstrates significant potential (6). The mineral composition of this material predominantly consists of dicalcium silicate (C_2S), supplemented by tetracalcium aluminate sulfate ($C_4A_3\check{S}$), and includes a small amount of tetracalcium iron aluminate (C_4AF) (7). Belite-ye'elimite cement exhibits substantial environmental and performance advantages over traditional silicate cements (8). Specifically, its manufacturing process can reduce CO_2 emissions by approximately 35% and limestone usage by 30%, showcasing significant environmental benefits (9). In terms of performance, this cement excels in early strength, permeability resistance, and corrosion resistance (10). Importantly, the production of this cement requires lower quality raw materials, facilitating the use of industrial solid waste as feedstock (11). The use of industrial solid waste not only reduces the consumption of natural resources but also enhances the environmental sustainability of the cement industry while effectively minimizing industrial waste emissions and aiding ecological protection. This aligns with the principles of sustainable development.

In recent years, numerous researchers have conducted extensive investigations into the production of belite-ye'elimite cement using industrial waste. For instance, Yao and colleagues successfully synthesized cement clinker from fly ash, limestone, and gypsum, demonstrating excellent early strength, durability, and frost resistance (12). Hou et al utilized electrolytic manganese slag, kaolin, and fly ash as raw materials, achieving a compressive strength of 65 MPa after 56 days (13). Gallardo et al produced cement clinker with a 28-day compressive strength of 47 MPa using aluminum slag, fluorogypsum, and limestone (14). Yanze et al employed marble waste as a calcium source to synthesize clinker, achieving a compressive strength of 21 MPa within a day (15). Zhang et al used phosphogypsum as a sulfur source to also produce high-performance cement clinker (16). Other researchers have prepared belite-ye'elimite cement clinker using industrial wastes such ash and slag waste, desulfurization petroleum coke slag, aluminum-rich sludge, recycled alumina scrap, aluminum ash, and limestone tailings (17-21). Test results have shown that these clinkers demonstrate good performance. Although significant progress has been made in the preparation of belite-ye'elimite cement using industrial waste, several challenges persist. Firstly, while most existing research focuses on partially substituting natural materials with solid waste, there is a lack of comprehensive studies on clinker preparation entirely from solid waste. This limitation could impede the efficient resource utilization of industrial waste and the low-carbon transition of the cement industry. Secondly, current studies predominantly focus on the mechanical properties and hydration characteristics of clinkers, with insufficient exploration into the mineral formation process during cement clinker production. Revealing the patterns of mineral changes and elucidating the mechanisms of mineral formation are critical for controlling clinker quality, optimizing clinker performance, and enhancing clinker calcination processes to reduce energy consumption (22, 23). Therefore, in-depth research into the mineral formation process of clinkers is essential for further advancing the sustainable development of the cement industry.

Addressing the outlined issues, this study utilized bulk industrial waste materials, including coal gangue (CG), carbide ash (CA), desulfurization gypsum (DG), and steel slag (SS), to prepare all-solid-waste belite-ye'elimite cement (BSAC) clinker. A diverse array of analytical techniques, including free calcium oxide (f_{CaO}), Fourier-transform infrared spectroscopy (FTIR), X-ray diffraction (XRD), scanning electron microscopy (SEM), and thermogravimetric-differential scanning calorimetry (TG-DSC), were employed to thoroughly investigate the mineral formation process in the clinker. Furthermore, the mechanical properties and environmental benefits of the synthesized clinkers were evaluated to ascertain their practical application feasibility. The objective is to provide valuable reference data for preparing BSAC clinker using CA, CG, SS, and DG, thereby facilitating the efficient resource utilization of industrial waste and the sustainable development of the cement industry.

2. MATERIALS AND EXPERIMENTAL METHODS

2.1. Materials

The used raw materials for preparing BSAC clinker include carbide ash (CA), coal gangue (CG), steel slag (SS), and desulfurization gypsum (DG), among which CG, DG and CA were obtained from Jungar area, SS was

provided by Baotou Steel Group. The composition and content of the oxides in materials were analysed by conducting X-ray fluorescence spectrum measurements (Table 1). The phase composition of the raw materials was analyzed by X-ray diffraction, as shown in Figure 1.

Table 1. Oxide composition of materials (wt. %).

Materials	Fe_2O_3	CaO	SiO_2	Al_2O_3	MnO	Cr_2O_3	MgO	TiO_2	SO_3	loss	∑
CA	0.05	74.96	0.63	0.22	/	/	/	/	/	23.97	99.83
CG	0.11	0.09	42.75	38.84	/	/	0.03	0.70	0.27	17.01	99.80
SS	26.30	33.76	16.93	7.11	2.55	2.18	3.74	0.55	0.83	4.37	98.32
DG	/	32.49	/	/	/	/	/	/	46.42	20.89	99.80

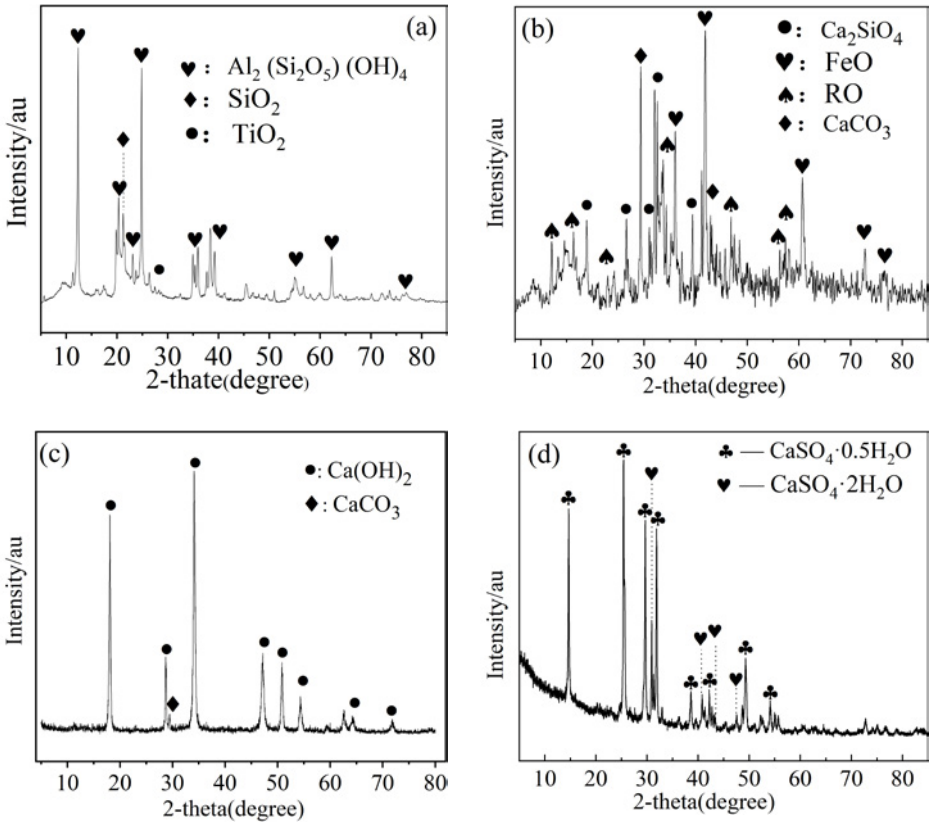

Figure 1. XRD spectra of raw materials (a) coal gangue, (b) steel slag, (c) carbide slag, (d) desulfurization gypsum.

2.2. Raw material ratio and preparation of the BSAC clinker

2.2.1. Raw material ratio

In the test, the design idea of the mineral composition of the BSAC clinker was to calcine silica in CG and SS to generate C_2S by carrying out a series of chemical reactions, whereas alumina was used in CG to generate C_4AF and $C_4A_3\check{S}$ through a series of chemical reactions. The calculation of the raw material ratio follows the improved Bogue method (24). The calculation formula is shown in Equations [1-5], and the raw material ratio is presented in Table 2.

$$W(CaO) = 0.6512W(C_2S) + 0.3762\ W(C_4A_3\check{S}) + 0.4616\ W(C_4AF) \quad [1]$$

$$W(SiO_2) = 0.3488W(C_2S) \quad [2]$$

$$W(Al_2O_3) = 0.5106W(C_4A_3\check{S}) + 0.2098W(C_4AF) \quad [3]$$

$$W(Fe_2O_3) = 0.33W(C_4AF) \quad [4]$$

$$W(SO_3) = 0.1311W(C_4A_3\check{S}) \quad [5]$$

Table 2. Oxide components and ration of materials (wt.%).

Group	Oxide composition					Raw materials			
	CaO	SiO_2	Al_2O_3	Fe_2O_3	SO_3	CA	CG	SS	DG
BSAC	53.99	19.41	16.75	2.86	6.69	47.9	32.38	8.42	11.31

2.2.2. Preparation of BSAC clinker

The materials were mixed in proportion, ground with a test mill, and passed through 200 mesh screen. Then, pressed the ground raw materials into round cakes with a diameter of 60 mm and a thickness of 5 mm. Finally, the round cakes were placed into a high-temperature furnace for calcination (air atmosphere), and the furnace temperature increased at a rate of 10 °C/min. After the furnace temperature reached the set temperature, the test cake was calcined for 40 minutes. It was then removed and cooled in ambient air. Once cooled to room temperature, the BSAC clinker was obtained, sealed, and stored to prevent moisture absorption or contamination. The temperature values set were 700 ºC, 800 ºC, 900 ºC, 1000 ºC, 1100 ºC, 1200 ºC, 1260 ºC, 1320 ºC, and 1350 ºC, respectively.

2.3. Preparation of BSAC

BSAC clinker and desulfurization gypsum are mixed and ground in a mass ratio of 96:4 and passed through a 200-mesh square sieve to obtain BSAC. The particle size distribution of BSAC is shown in Figure 2, with a particle size range of 0.12μm to 105μm and an average particle size of 46μm. The chemical compositions of BSAC are shown in Table 3.

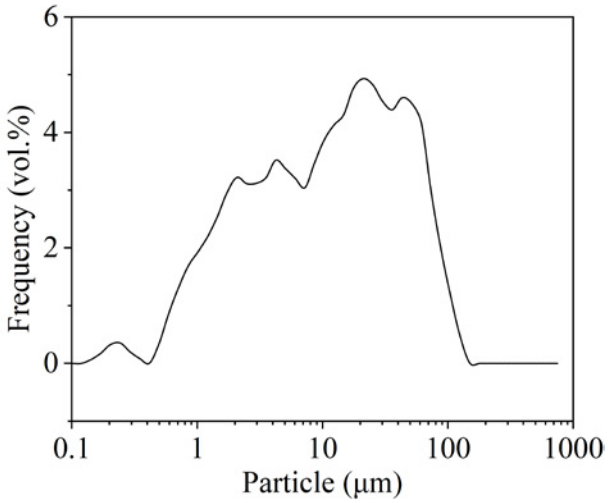

Figure 2. Particle size distribution of BSAC.

Table 3. Chemical composition of BSAC (wt. %).

Group	CaO	SiO_2	Al_2O_3	Fe_2O_3	SO_3	MnO	MgO	TiO_2	Na_2O	loss	∑
BSAC	54.54	18.16	16.42	2.80	6.83	0.09	0.16	0.03	0.11	0.79	99.93

2.4. Experimental methods

2.4.1. Free calcium oxide

In this experiment, the content of f_{CaO} in BSAC clinker was determined by the ethylene glycol method (25). First, the clinker was mixed with the ethylene glycol extraction solution, and the mixture was extracted by using a Ca-5-f_{CaO} analyzer for 5 min. After the extraction process, the mixture was titrated with a benzoic acid titration solution until the mixture became colorless. Repeated the above test steps until the mixture after extraction was no longer red. The calculation of f_{CaO} is based on Equations [6 -7]:

$$T_{cao} = \frac{1000 \times G_1}{V_1} \quad [6]$$

$$f_{cao}\% = \frac{T_{cao} \times V_2 \times 100}{G_2 \times 1000} \quad [7]$$

The T_{CaO} represents the titer of benzoic acid titration solution to CaO (mg/ml), G_1 is the mass of calcium oxide (g), V_1 denotes the volume (ml) consumed by the benzoic acid titration solution when titrating the calcium oxide mixed solution, f_{CaO} refers to the content of the free calcium oxide in clinker, V_2 is the volume (ml) of benzoic acid titrant consumed when titrating the clinker mixed solution, and G_2 stands for the mass (g) of the clinker.

2.4.2. Phase analysis

The phase analysis of the minerals in the clinker was carried out by using the x-ray diffraction (XRD) (X'Pert powder, Netherlands) test method. More specifically, when the clinker sample was measured, the sample was ground by a planetary ball mill. Next, the XRD measurements were carried out. During XRD testing, Cu Kα radiation (40 kV, 40 mA) was used, along with a graphite monochromator and a flat sample holder. The scanning range was from 5° to 85° (2θ), with a scanning speed of 0.02°/second. Sample rotation was enabled during the data collection process.

2.4.3. Fourier transform infrared spectrum

The Fourier transform infrared spectrum **(**FTIR) (IRTracer-100, Japan) analysis can characterize the minerals in clinker from the molecular structure level. Before the measurements, the clinker was ground by using a planetary ball mill. During the measurements, potassium bromide and clinker were mixed, ground and tableted at a ratio of 100:1, and then measured by FTIR. In FTIR testing, the scanning range was from 4000 cm^{-1} to 400 cm^{-1}, with a resolution of 2 $cm^{-1}$and 45 accumulative scans.

2.4.4. Thermogravimetric comprehensive analysis

The thermogravimetric comprehensive analysis (STA 449 F5 Jupiter, Germany) can reflect the relationship between the sample mass and temperature, as well as the endothermic and exothermic conditions of the sample at different temperature values. Before the thermogravimetric measurements, the raw material was ground by using a planetary ball mill. Then, about 35 mg of the raw material was taken for the thermogravimetric test. In thermogravimetric testing, the heating rate was set to 10 °C/min, with a nitrogen flow rate maintained at 50ml/min. Data were recorded at a frequency of one data point per degree Celsius.

2.4.5. Scanning electron microscope

The micromorphological of the BSAC clinker minerals was analyzed by scanning electron microscope (FEI QUANTA 650, USA). Before the measurement, the powder or block clinker was fixed on the conductive adhesive, gold was spayed, and then photographed by SEM and analyzed by X-ray energy dispersive spectrometer (EDS).

2.4.6. Compressive strength of BSAC

The mechanical properties of BSAC were tested in strict accordance with the "Sulphoaluminate Cement" (GB/T 20472-2006) standard.

3. RESULT AND DISSCUSSION

3.1 Appearance characteristics

Figure 3 illustrates the appearance characteristics of BSAC clinker at varying calcining temperatures. At 700-1100 ºC, the clinker displays a light gray color, maintains its volume, and possesses a soft texture, making it easily crushable. This is attributed to the lower calcining temperature, which prevents liquid phase formation, leading to mineral generation via solid-phase reactions. In contrast, at 1200-1320 ºC, notable changes occur in the clinker's color, volume, and texture. At 1200 ºC, the clinker slightly shrinks and hardens, indicating liquid phase presence

during calcination. This liquid phase aids in ion diffusion, facilitating mineral crystallization and growth (26). As the temperature rises, the clinker darkens, and its volume decreases significantly. This is due to the increasing liquid phase, enhancing the development of C_2S, $C_4A_3\check{S}$, and C_4AF crystals (27).

At a calcining temperature of 1350 ºC, the clinker undergoes significant shrinkage and becomes relatively hard. This results from an excessive liquid phase caused by the high temperature. Such a surplus increases the liquid's viscosity and surface tension, impeding ion diffusion and hampering mineral crystal formation and growth (28). Moreover, excessively high temperatures can cause the decomposition of active minerals in the clinker.

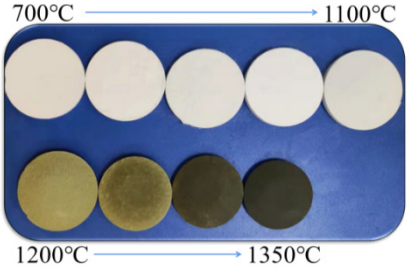

Figure 3. Appearance characteristics of clinker at different calcining temperature values.

3.2. Analysis of clinker maturity based on fCaO

The content of the f_{CaO} in clinker can directly reflect the formation rate of minerals in clinker and the maturity of the clinker in different calcining temperature ranges. The f_{CaO} content in the clinker is shown in Figure 4.

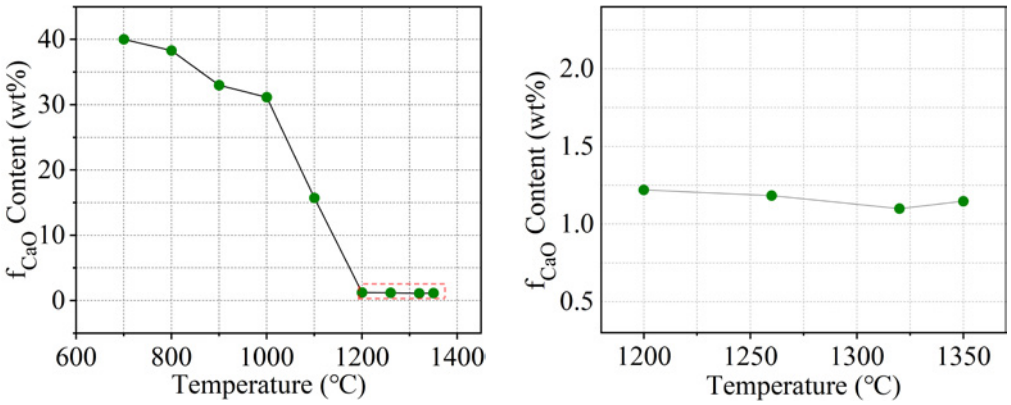

Figure 4. Content of the fCaO in clinker at different calcining temperature values.

It is evident that the f_{CaO} content in clinker decreases as the calcining temperature increases, indicating a gradual maturation of the clinker. The calcining temperature can be categorized into three stages: 700-1000 ºC, 1000-1200 ºC, and 1200-1350 ºC. At 700-1000 ºC, the f_{CaO} content changes minimally, with only an 8.8% decrease at 1000 ºC compared to 700 ºC. This suggests a slow mineral formation rate in this range, predominantly comprising transitional minerals. In contrast, the 1000-1200 ºC range shows a substantial reduction in f_{CaO} content, from 31.1% at 1000 ºC to 1.2% at 1200 ºC, implying complete reaction of f_{CaO} and significant mineral formation. Above 1200 ºC, changes in fCaO are minimal, indicating that the final minerals (C_2S, C_4A_3) have formed by the time the temperature reaches 1200 ºC. When the calcining temperature was 1350 ºC, the content of the f_{CaO} increased, which should be due to the decomposition of $C_4A_3\check{S}$ to produce $CaSO_4$, which continued to decompose to produce calcium oxide (Equation [8]) (29).

$$Ca_4Al_6SO_{16} \rightarrow Ca_3\,Al_2O_6 + SO_2 + CaO \qquad [8]$$

3.3. Phase analysis of minerals

X-ray diffraction measurements were used to analyze the mineral phases in clinker, as illustrated in Figure 5. The analysis of Figure 5a indicates minimal changes in the mineral composition of clinker at calcining temperatures be-

tween 700-900 ºC. The composition primarily includes CaO, calcium sulfate (CŠ), and various transition minerals like gehlenite (C_2AS), anorthite (CAS_2), dodecalcium heptaaluminate ($C_{12}A_7$), and grossular (C_3AS_3). Transition minerals often display weak XRD diffraction peaks due to their low content or underdeveloped crystal structures.

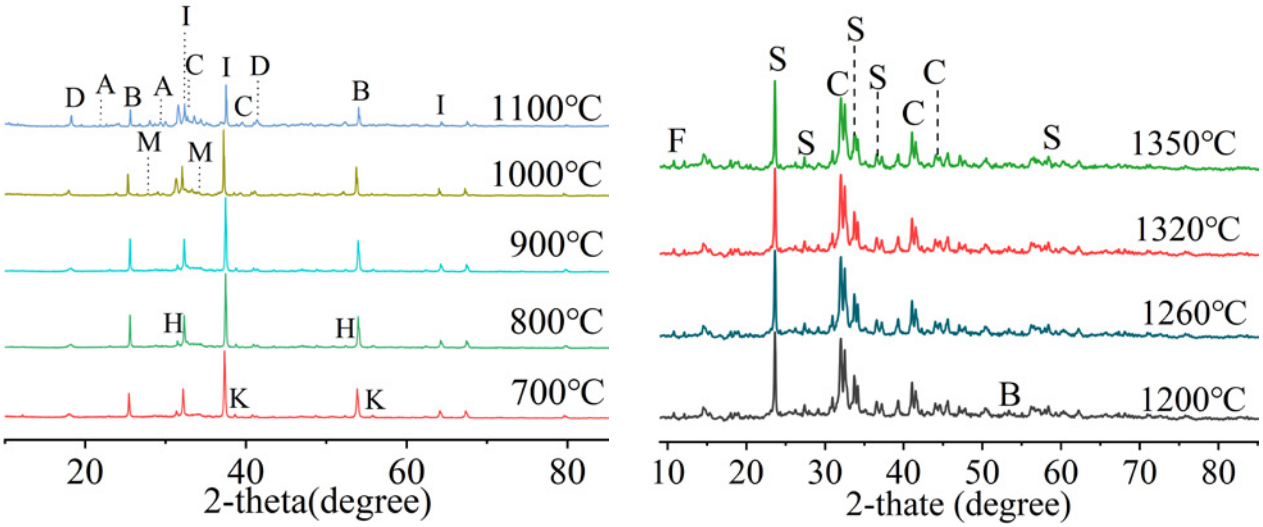

Figure 5. Left: XRD patterns of clinker calcined at 700–1100 °C, A- CAS^2, B- CŠ, C- C^2S, D- $C^{12}A^7$, H- C^2AS, I- CaO, K- C^3AS^3, M- $C^5S^2Š$. Right: XRD patterns of clinker calcined at 1200–1350 °C, B- CŠ, C- C^2S, F- C^4AF, S- $C^4A^3Š$.

Post-calcination, kaolinite in CG and calcium hydroxide in CA contribute to the formation of metakaolinite (Equation [9]) and CaO (Equation [10]), which are highly reactive. These substances interact to produce C_2AS (Equation [11]) and CAS_2 (Equation [12]) through solid-phase reactions, as documented in references (30, 31). Additionally, $C_{12}A_7$ (Equation [13]) forms through the reaction of amorphous Al_2O_3, derived from CG, with CaO (32). C_3AS_3, a metastable mineral, originates from the decomposition of CG and CA (30).

At a calcining temperature of 1000 ºC, new minerals, C_2S (Equation [14]) and calcium sulphosilicate ($C_5S_2Š$) (Equation [15]), were observed in the clinker (33). C_2S formed from the reaction of amorphous SiO_2, originating from CG, with CaO (32). $C_5S_2Š$ resulted from the solid-phase reaction between C_2S and CŠ. As the temperature increased to 1100 ºC, the XRD diffraction peaks for CaO and CŠ diminished, while those for C_2S, C_2AS, CAS_2, $C_{12}A_7$, and other minerals intensified significantly. This suggests an increased mineral formation rate between 1000-1100 ºC, leading to an abundance of transition minerals, aligning with previous analyses.

At 1200 ºC, the mineral composition in the clinker underwent significant changes, as depicted in Figure 5b. The XRD peaks of CaO, CŠ, and transition minerals were replaced by those of C_2S, $C_4A_3Š$, and C_4AF. This indicates that between 1100-1200 ºC, transition minerals either decomposed or reacted with CaO and CŠ, forming substantial amounts of C_2S and $C_4A_3Š$.

Through the analysis, it was found that the minerals in the clinker may have the following reactions (Equations [16-20]) (33-35). When the temperature exceeds 1200 °C, the XRD patterns show minimal changes, with the diffraction peaks primarily dominated by dicalcium silicate C_2S and $C_4A_3Š$.

$$Al_2Si_2O_7 \cdot 2H_2O \rightarrow Al_2Si_2O_7 + 2H_2O \quad [9]$$

$$Ca(OH)_2 \rightarrow CaO + H_2O \quad [10]$$

$$Al_2Si_2O_7 + 2\,CaO \rightarrow Ca_2Al_2SiO_7 + Si_O2 \quad [11]$$

$$Ca_2Al_2SiO_7 + Al_2Si_2O_7 + SiO_2 \rightarrow 2\,CaAl_2Si_2O_8 \quad [12]$$

$$7\,Al_2O_3 + 12CaO \rightarrow Ca_{12}Al_{14}O_{33} \quad [13]$$

$$SiO_2 + 2\,CaO \rightarrow Ca_2SiO_4 \quad [14]$$

$$2Ca_2SiO_4 + CaSO_4 \rightarrow Ca_5SiO_8(SO_4) \quad [15]$$

$$Ca_5SiO_8(SO_4) \rightarrow 2Ca_2SiO_4 + CaSO_4 \quad [16]$$

$$3Ca_2Al_2SiO_7 + CaSO_4 + 3CaO \rightarrow Ca_4Al_6SO_{16} + 6Ca_2SiO_4 \quad [17]$$

$$3CaAl_2Si_2O_8 + CaSO_4 + 8CaO \rightarrow Ca_4Al_6SO_{16} + 6Ca_2SiO_4 \quad [18]$$

$$3Ca_3Al_2Si_3O_{12} + CaSO_4 + 12CaO \rightarrow Ca_4Al_6SO_{16} + 9Ca_2SiO_4 \quad [19]$$

$$Ca_{12}Al_{14}O_{33} + 5Al_2O_3 + 4CaSO_4 \rightarrow 4Ca_4Al_6SO_{16} \quad [20]$$

3.4. Molecular structure analysis of minerals

The acquired infrared spectra of clinker at different calcining temperature values are shown in Figure 6a.

Since many minerals exist in the clinker, the infrared spectra of all minerals will overlap, which is not conducive to their analysis. Thus, the second derivative curve of the infrared spectrum was drawn (Figure 6b).

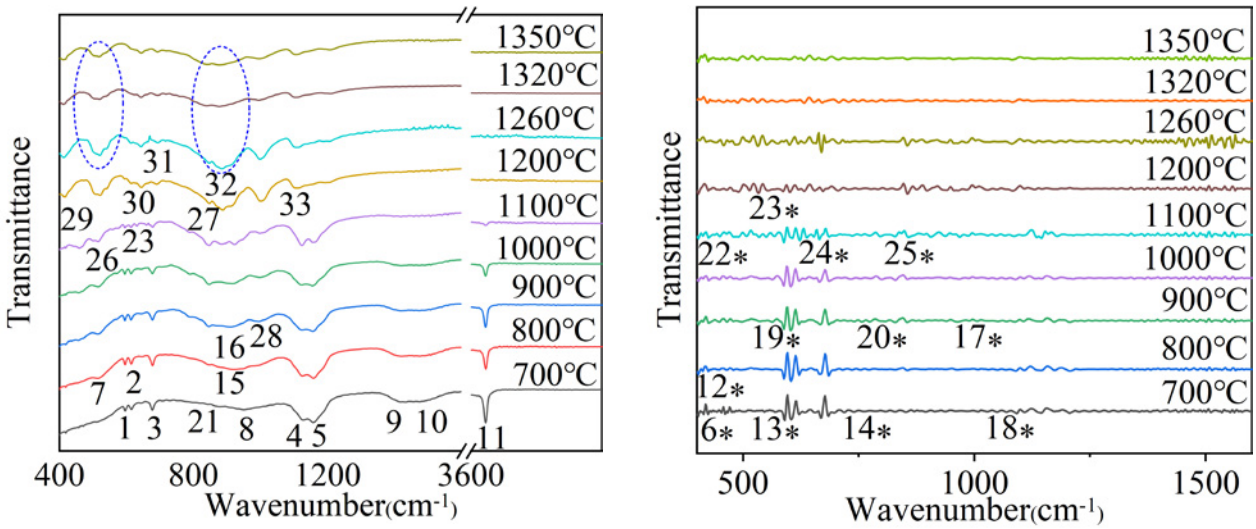

Figure 6. Left: infrared spectra of clinker calcined at various temperatures. Right: second-derivative curves of the infrared spectra.

In the data analysis from Figure 6a, an absorption band at 3640 cm^{-1} in the clinker's infrared spectrum was observed between 700-1100 ºC, attributed to the hydroxy(O-H) asymmetric stretching vibration (36). This indicates the presence of $Ca(OH)_2$ in the clinker, formed by CaO reacting with atmospheric water. Notably, the $Ca(OH)_2$ content decreases as the calcining temperature increases, aligning with previous analyses. Additionally, a broad absorption band at 1350-1500 cm^{-1}, related to C-O bonds in $CaCO_3$ (37), suggests its formation from $Ca(OH)_2$ and atmospheric CO_2. The characteristic absorption bands of CŠ at 595, 613, 679, 1120, and 1154 cm^{-1}, caused by the (SO_4) tetrahedral group's bending and asymmetric stretching vibrations, were stable between 700-1000 ºC (38, 39). However, at 1100 ºC and 1200 ºC, significant changes in these bands indicate CŠ's involvement in forming other minerals.

In the 700-1100 ºC range, the clinker's spectrum revealed two broad infrared absorption regions at 420-550cm^{-1} and 900-1250 cm^{-1}, as shown in Figure 6a. These regions correspond to the bending vibrations of Si-O and Al-O in silica aluminate and the asymmetric stretching vibrations of Si-O-Si and Si-O-Al. Notably, these regions include the spectral bands of C_3AS_3 (435* cm^{-1}, 514cm^{-1}, and 950cm^{-1}) (39-40), C_2AS (472*cm^{-1}, 558*cm^{-1}, 746*cm^{-1}, and 920cm^{-1}) (39-41), and CAS_2 (908cm^{-1}, 997*cm^{-1}, and 1059*cm^{-1}) (42), which vary with calcining temperature. This variation suggests the ongoing development of silica-aluminate minerals within this temperature range. Additionally, the presence of the $C_{12}A_7$ band (573* cm^{-1}, 783* cm^{-1}, and 848 cm^{-1}) (43) in this range, increasing in intensity with temperature, indicates the continuous development of $C_{12}A_7$. At 1100 ºC, the spectrum shows the $C_5S_2Š$ band (630 cm^{-1}, 661* cm^{-1}, and 836* cm^{-1}), related to the bending of (SO_4) and stretching of (SiO_4) groups (44). The formation of $C_5S_2Š$, consuming CŠ, explains the decrease in CŠ›s absorption band intensity.

At a calcining temperature of 1200 ºC, the clinker's infrared spectrum underwent significant changes. The absorption bands of CŠ and transition minerals nearly vanished, replaced by bands of C_2S and $C_4A_3Š$. Specifically, C_2S bands appeared at 460-570 cm^{-1} and 960-1070 cm^{-1}, with notable bands at 520 and 543 cm^{-1} due to the (SiO_4) group's out-of-plane bending vibrations (45, 46), and at 995 cm^{-1} from its asymmetric stretching vibration. The $C_4A_3Š$ band, characterized by the (AlO_4) group's asymmetric contraction (413 cm^{-1}), bending (884 cm^{-1}), and coupling stretching vibrations with (SO_4) (644, 692 cm^{-1}), and (SO_4) group's asymmetric stretching (1103 cm^{-1}), also emerged (45). Notably, at higher temperatures of 1320 ºC and 1350 ºC, these bands became broad and weak, as shown in Figure 6a. This broadening and weakening, often associated with crystal damage or symmetry deterioration, suggest that the dicalcium silicate's crystals might undergo melting at these temperatures, leading to structural damage or symmetry loss (47).

Figure 7 depicts the infrared absorption peaks of C_2S and $C_4A_3Š$. As can be ascertained, with the increase in the calcining temperature, the infrared absorption peaks of C_2S and $C_4A_3Š$ not only changed in intensity, but also shifted in position. Hence, it can be argued that the crystal structures of both C_2S and $C_4A_3Š$ maintain continuous development with the increase of the calcining temperature, which is consistent with the above analytical findings.

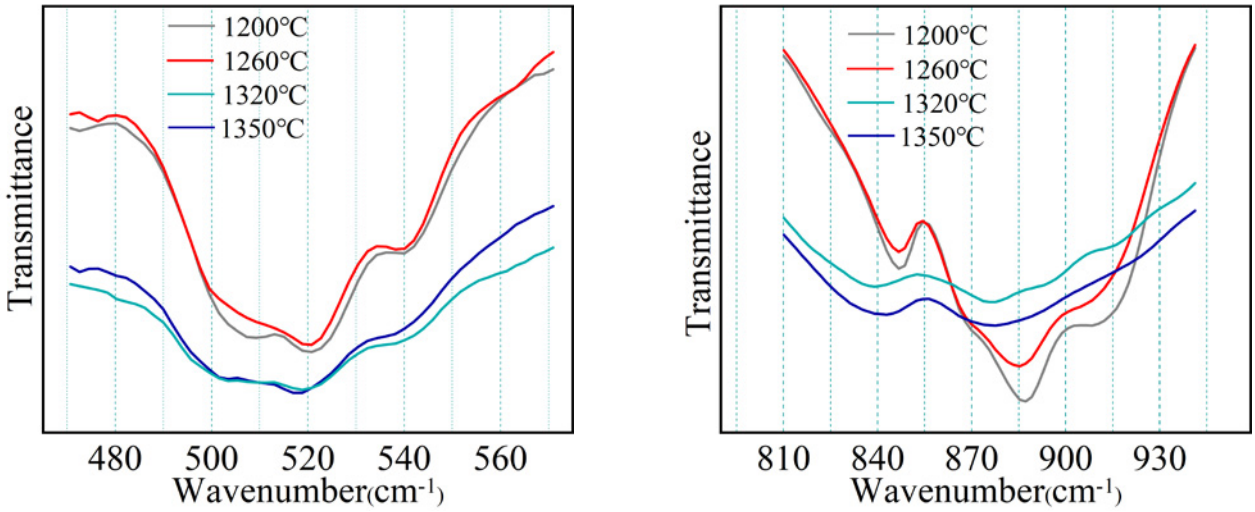

Figure 7. Infrared absorption of dicalcium silicate and tetracalcium sulfoaluminate.

3.5. Thermal reaction characterization analysis of minerals

Figure 8 presents the TG-DSC curve of the raw material, revealing distinct endothermic peaks at 156 ºC, 500 ºC, 540 ºC, and 710 ºC, all corresponding to mass losses.

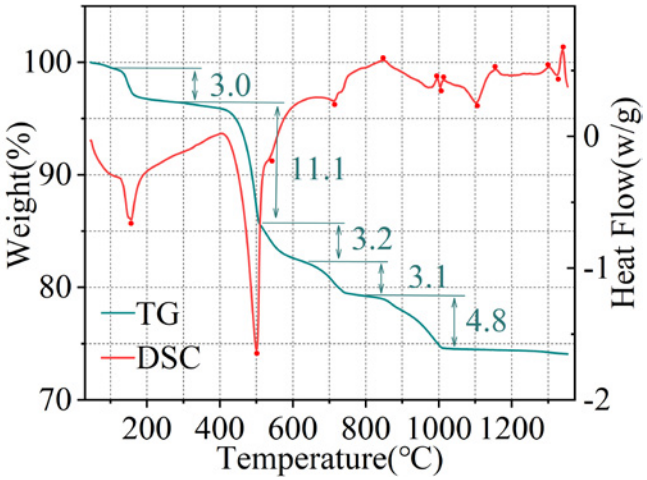

Figure 8. TG-DSC curves.

These peaks result from the decomposition of gypsum dihydrate, calcium hydroxide, kaolinite, and calcium carbonate, leading to the production of active CaO, Al_2O_3, and SiO_2 (48-50). Combined with the analysis results of the XRD measurements and Fourier infrared spectroscopy, it can be seen that there should be a small number of intermediate minerals in the temperature range of 540-710 ºC. As the temperature increases to 847-1013 ºC, DSC shows broader absorption bands, suggesting ongoing development of transition minerals. The mass loss around this range is likely due to CŠ decomposition (51). Notably, a small endothermic peak at 1004 ºC, marking the formation of C_2S (47), implies its successful formation around 1000 ºC.

The DSC curve records two broad absorption bands between 1013-1302 ºC, without significant mass loss on the TG curve, indicating the formation of numerous minerals. This is consistent with the earlier analysis, pointing to a significant creation of transition minerals in the 1013-1156 ºC range. In the temperature range of 1156-1302 ºC, the transition minerals will decompose or participate in the reaction to generate the final minerals (C_2S, $C_4A_3Š$, and C_4AF), the transition minerals will gradually disappear, and the final minerals will be generated and continue to develop. With the further increase in the temperature, the DSC curve shows an endothermic peak at 1324 ºC, which may be due to the solid phase melting in the system. When the temperature is higher than the value of 1340 ºC, the system exhibited a continuous endothermic state accompanied by mass loss, which should be caused by the decomposition of $C_4A_3Š$.

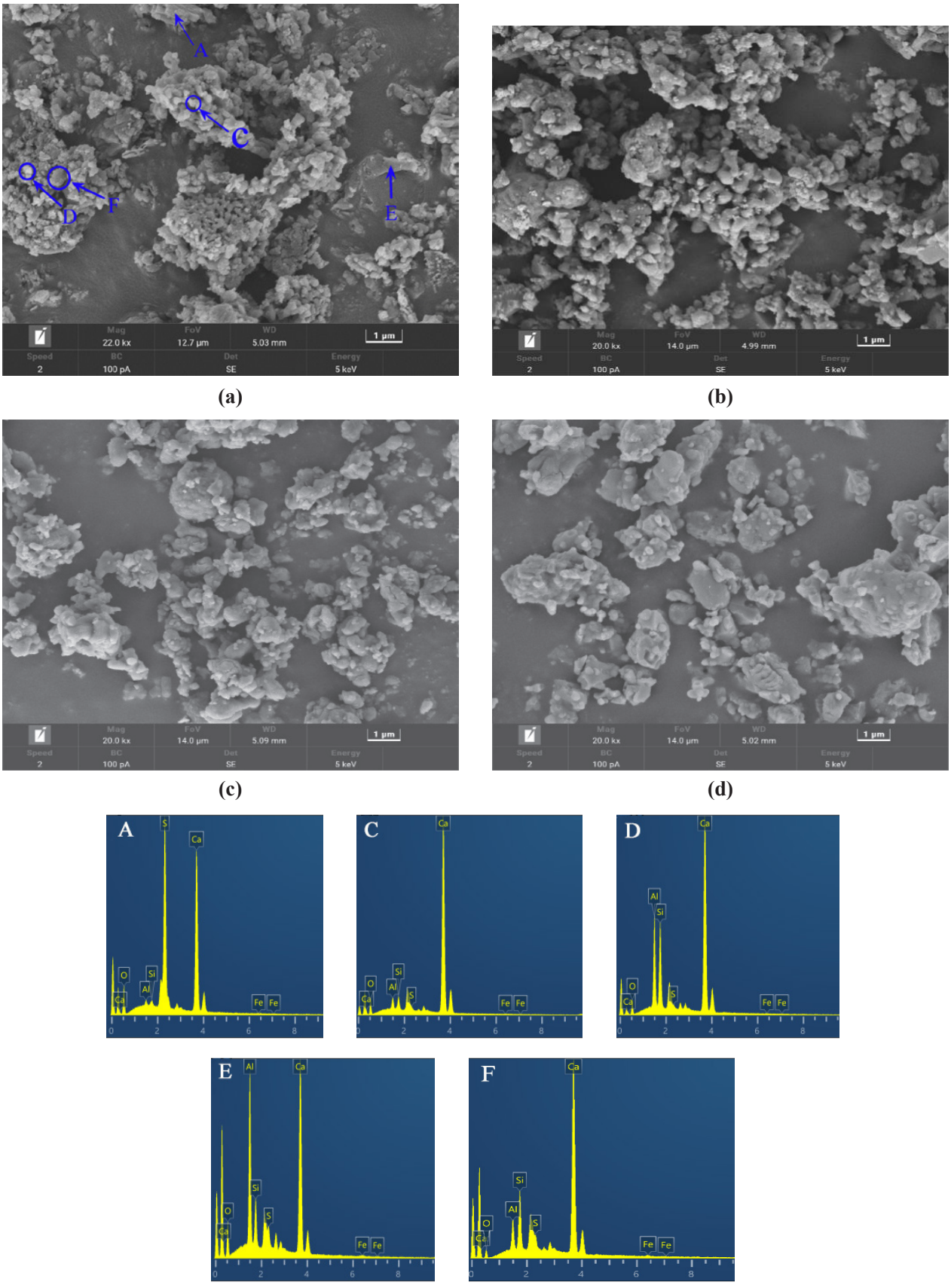

Figure 9. Micromorphology and EDS analysis of the clinker at different calcining temperatures (a: 700ºC, b: 900ºC, c: 1000ºC, d: 1100ºC). A-CŠ; C-CaO; D, E and F-silica aluminate.

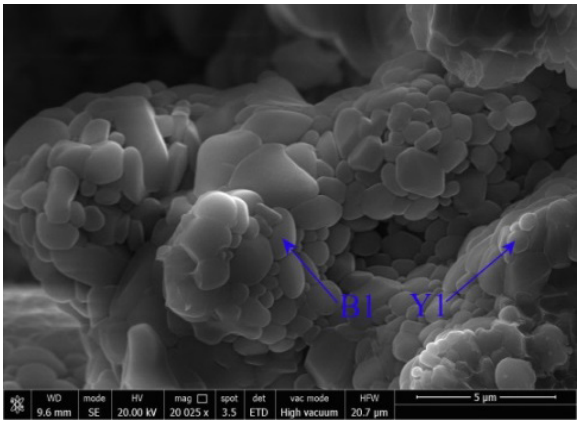

Figure 10a. 1200 ºC

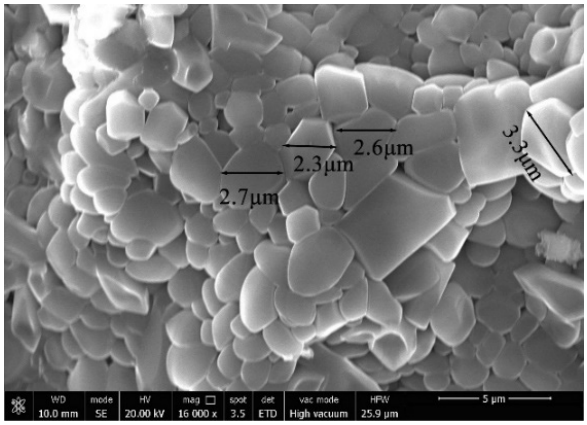

Figure 10b. 1260 ºC

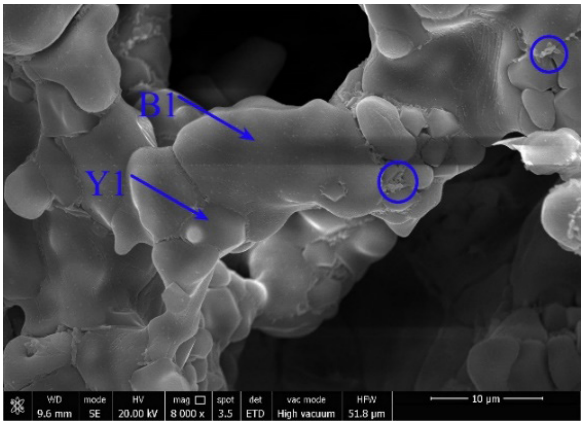

Figure 10c. 1320 ºC

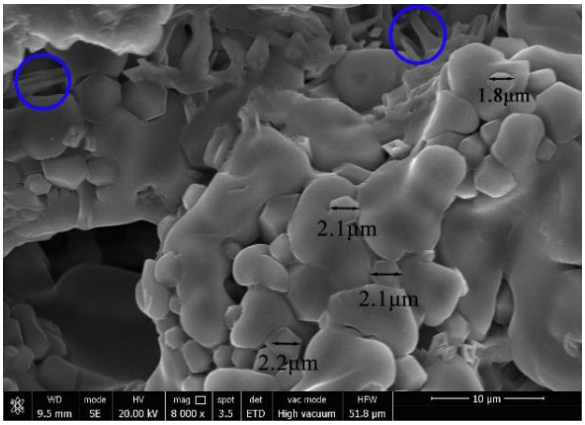

Figure 10d. 1350 ºC

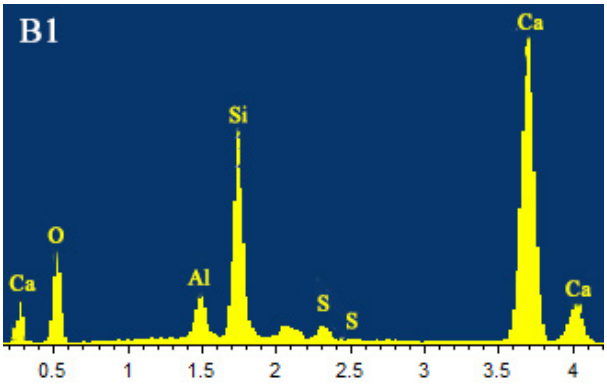

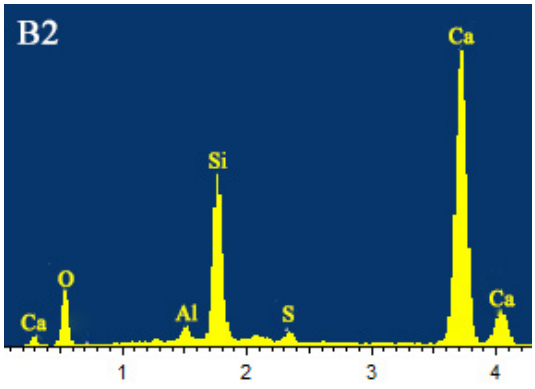

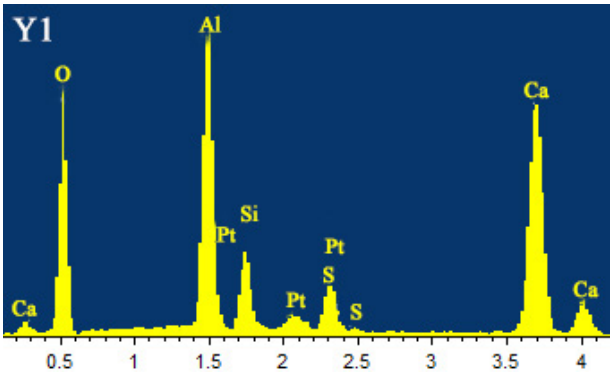

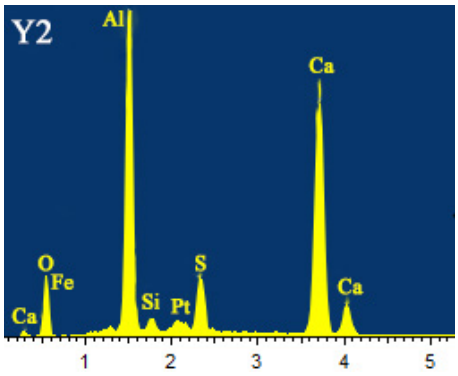

Figure 10. Micromorphology and EDS analysis of the clinker at different calcining temperature values (a: 1200ºC, b: 1260ºC, c: 1320ºC, d: 1350ºC). B1- C_2S, Y1- $C_4A_3\check{S}$, B2- C_2S, Y2- $C_4A_3\check{S}$.

3.6. Mineral microstructure analysis

The micromorphology and EDS analysis of the clinker at different calcining temperature values are shown in Figures 9 and 10.

In analyzing the data, it was noted that at 700 ºC, the clinker's minerals were predominantly spherical CaO, with minor rod-shaped CŠ and transition minerals. (aluminosilicate). Due to the complex composition of the raw meal, a small number of impurity elements will appear in the EDS analysis of the minerals. At 900 ºC, the CaO minerals, now larger, remained predominant. However, as the temperature rose, spherical CaO's size and proportion diminished, while those of transition minerals increased, particularly at 1100 ºC, marking a significant shift. This suggests that between 700-1100 ºC, transition minerals evolve rapidly, especially in the 1000-1100 ºC range.

At 1200 ºC, the transition minerals and CaO were almost entirely replaced by hexagonal plate-shaped $C_4A_3Š$ and elliptical C_2S. SEM-EDS analysis revealed these crystals contained more impurity ions and were smaller, indicating their immature development. As the calcining temperature reached 1260 ºC, the crystals of $C_4A3Š$ and C_2S grew in size, with more defined contours.

At 1320 ºC, needle-like C_4AF emerged in the clinker, accompanied by the melting of C_2S. At this stage, C_2S crystals exhibited an irregular morphology, and the crystal size increased. EDS analysis indicated a reduction in impurity ions in the crystals at this stage, suggesting continuous development of $C_4A_3Š$ and C_2S between 1200-1320 ºC. This aligns with the observed changes in the XRD main diffraction peaks of C_2S and $C_4A_3Š$ with temperature increase. At 1350 ºC, the rod-shaped C_4AF crystals enlarged, likely due to an excess of liquid phase in the clinker. Interestingly, the size of $C_4A_3Š$ crystals decreased, possibly due to decomposition at this high temperature, aligning with the earlier analysis.

4. MECHANICAL PROPERTY

BSAC is produced by grinding clinker (1260 ºC) with desulfurized gypsum in a 96:4 ratio. Its compressive and flexural strengths are shown in Figures 11 and 12, alongside those of SAC-52.5 mortar as specified by GB 20472-2006 for comparison.

Analysis reveals that the compressive strength of BSAC mortar increases with curing age, without any strength retrogression. The development of compressive strength in BSAC mortar is mainly concentrated in the early hydration period. The compressive strength at a curing age of 1 day reaches 44 MPa, primarily attributed to the presence of highly reactive $C_4A_3Š$ in BSAC. At 7 and 28 days, the compressive strength advances to 53 MPa and 55 MPa, respectively. Similarly, flexural strength shows a consistent trend, starting at a high of 8.3 MPa after 1 day and progressing to 8.9 MPa and 9.1 MPa at 7 and 28 days, respectively.

As per Figures 11 and 12, BSAC mortar's performance meets the standards set for SAC-52.5 mortar by GB 20472-2006.

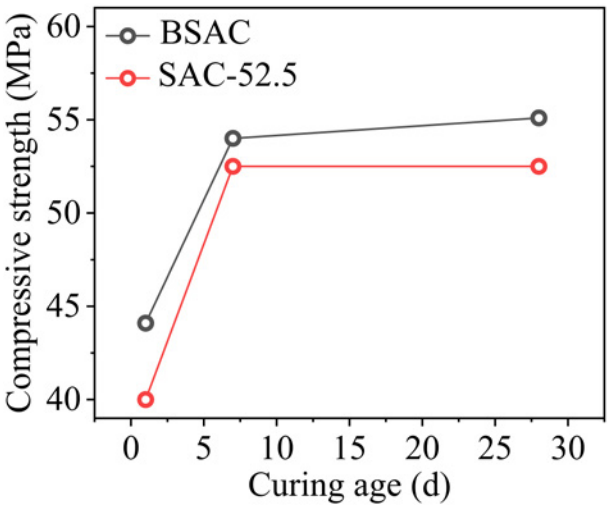

Figure 11. The compressive strength of BSAC.

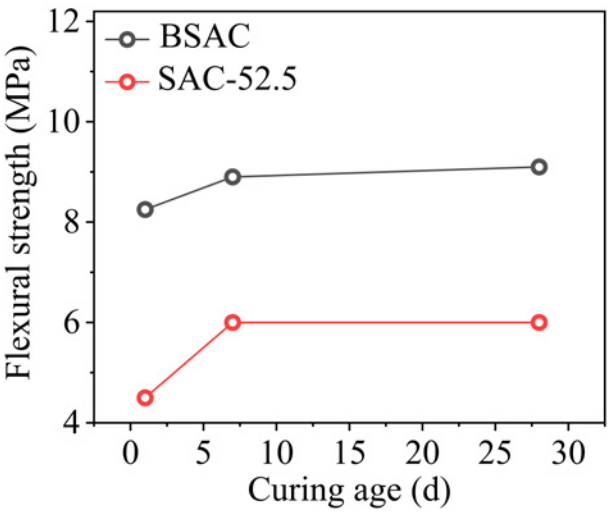

Figure 12. The flexural strength of BSAC.

5. BENEFIT ANALISIS OF BSAC CLINER

The preparation of PC clinker is a high consumption and high pollution process, while BSAC clinker preparation is characterized by lower consumption and emissions. This section will analyze the advantages of using CA, CG, DG, and SS in BSAC clinker production, focusing on resource utilization, energy consumption, and carbon emissions. The relevant data are presented in Table 4.

Table 4. Energy consumption and carbon emissions of producing 1t of BSAC and PC clinker.

Group		Process					
		Mining [a]	**Transporting [b]**	**Preparation [c]**	**Calcination [d]**	**Grinding [e]**	**Total**
BSAC	**Materials**	Kg/t BSAC	Km				
	Carbide ash	6.09 E+02	1E+02	/	/	/	/
	Coal gangue	4.12 E+02	1E+02	/	/	/	/
	Steel slag	1.07 E+02	1E+02	/	/	/	/
	Desulfurization gypsum	1.44 E+02	1E+02	/	/	/	/
	Raw coal	1.06 E+02	1E+02	/	/	/	/
	Energy source			/	/	/	/
	Raw coal (Kg)	6.27E-02	2.40E-01	1.64E+00	1.03E+02	5.51E-03	1.04E+02
	Crude oil (Kg)	1.78E-01	6.63E+00	8.44E-03	/	1.15E-04	6.81E+00
	Natural gas (m^3)	5.04E-04	3.97E-04	1.36E-02	/	8.90E-02	1.06E-01
	Electricity (Kw · h)	/	/	1.45E+01	2.81E+01	3.67E+01	7.93E+01
	Energy consumption (MJ)	8.79E+00	3.62E+02	2.38E+02	2.56E+03	5.17E+02	3.69E+03
	CO2(Kg)	6.81E-01	2.14E+01	2.28E+01	2.40E+02	4.91E+01	3.34E+02
PC	**Materials**	Kg/t PC	Km	/	/		
	Limestone	1.32 E+03	1E+02	/	/	/	/
	Clay	2.38 E+02	1E+02	/	/	/	/
	Iron	3.8 E+01	1E+02	/	/	/	/
	Energy consumption (MJ)	3.10E+02	3.31E+02	4.80E+02	2.77E+03	5.60E+02	4.45E+03
	CO2(Kg)	2.91E+01	2.46E+01	4.59E+01	7.94E+02	5.31E+01	9.47E+02

[a] Data Calculation— (52-58)
[b] Data Calculation— (52, 54-57, 59)
[c] Data Calculation — (52-62)
[d] Data Calculation — (52, 55-63)
[e] Data Calculation — (52, 54-59)

5.1. Analysis of natural resource benefit

CG, rich in silicon and aluminum, and CA, rich in calcium, are high-quality materials for BSAC clinker. Their use enhances solid waste utilization, reducing environmental impact and reliance on natural resources. In BSAC clinker production, solid waste utilization reaches 100% (Figure 12). In contrast, producing 1 ton of PC clinker consumes up to 1599 Kg of natural resources, including 1323 Kg of limestone (Figure 13).

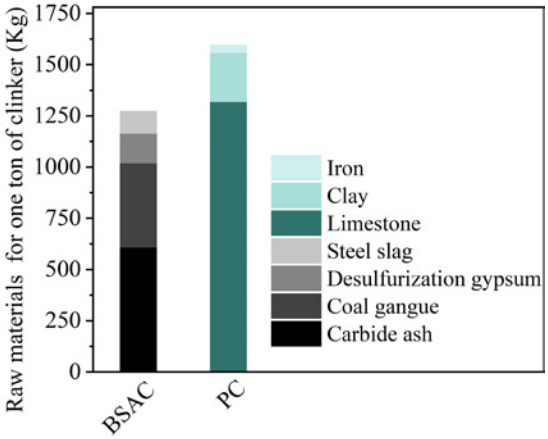

Figure 13. Materials required to produce 1t BSAC, PC clinker.

5.2. Analysis of energy consumption benefit

The energy consumption of PC clinker and BSAC clinker from the five stages of raw material mining, transportation, preparation, clinker calcination and grinding will be analysed here. The energy consumption in the whole preparation process is shown in Figure 14.

Figure 14 shows that BSAC clinker's energy consumption is lower than PC clinker at all stages. The substantial use of solid waste in BSAC clinker production contributes to significantly lower energy consumption, especially during the mining stage. For 1 ton of BSAC clinker, approximately 1272 Kg of raw material is needed, compared to 1599 Kg for PC clinker, reflecting a 20% reduction (52). This results in lower energy consumption for BSAC clinker during transportation. In the material preparation stage, energy consumption mainly arises from grinding. Since CA is already in powder form, BSAC clinker production requires less treatment, reducing energy usage compared to PC clinker. During calcination, BSAC clinker also consumes less energy due to its lower firing temperature (1200-1320 ºC) and the lower pyrolysis activation energy of $Ca(OH)_2$ in CA (130 KJ/mol) (64) compared to $CaCO_3$ in limestone (182 KJ/mol) (65). In the final grinding stage, BSAC clinker, containing less iron phase than PC clinker, is softer and easier to grind, further lowering energy consumption.

5.3. Analysis of carbon emission benefit analysis

The carbon emissions of the PC clinker and BSAC clinker at various stages are shown in Figure 15. As can be observed, the carbon emissions of the BSAC clinker in the raw material mining stage, transportation stage, preparation stage, and clinker grinding stage were reduced, and the carbon emission comes from the combustion of energy minerals. Therefore, the reduction of the carbon emissions in these stages can be attributed to the same arguments that were for the reduction of energy consumption, which was earlier discussed.

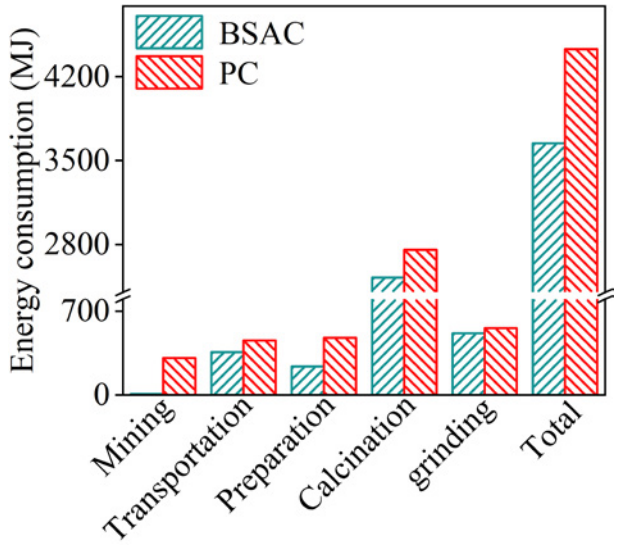

Figure 14. Energy consumption for producing 1t BSAC, PC clinker.

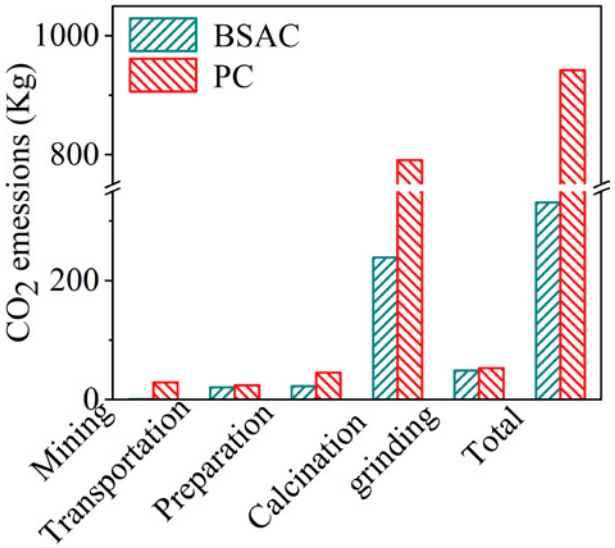

Figure 15. CO_2 emissions for producing 1t BSAC, and PC clinker.

A detailed analysis of Figure 15 shows that PC clinker emissions at Calcination stage reach 794 Kg, about three times higher than BSAC clinker. This difference is primarily due to the calcium materials used. In PC clinker, limestone ($CaCO_3$) is the main ingredient, decomposing into CO_2 during calcination, contributing significantly to emissions. In this stage, CO_2 from $CaCO_3$ decomposition in PC clinker is as high as 531 Kg (60), representing roughly 70% of its total emissions. Conversely, BSAC clinker uses CA ($Ca(OH)_2$), which decomposes into H_2O and CaO, resulting in a different emission profile. As far as CG and SS and DG are concerned, only a very small amount of $CaCO_3$ contained in SS will produce CO_2 after the calcination process. The carbon emission of the BSAC clinker in the calcination stage mostly originates from the combustion of energy.

6. CONCLUSIONS

In this study, the mineral formation in BSAC clinker systematically investigated, prepared using CA, CG, DG and SS, and tested its mechanical property. The BSAC clinker's advantages in terms of natural resource use, energy consumption, and carbon emissions were also analyzed. The key conclusions are:

1. At calcining temperatures between 700-1100 ºC, the clinker is mainly composed of transition minerals like anorthite, dodecacalcium heptaaluminate, grossular, and a notable amount of CaO. Around 1000 ºC, C_2S starts to form in small quantities. From 1100-1200 ºC, these transition minerals increasingly convert to C_2S and $C_4A_3\check{S}$, with the latter minerals becoming more dominant. Above 1200 ºC, the growth in size and structure of C2S and C4A3Š crystals is evident. Notably, at temperatures over 1320 ºC, needle-shaped C4AF crystals appear, and C2S crystals melt into irregular shapes. Beyond 1350 ºC, the clinker shows excessive liquid phase formation and decomposition of C4A3Š. Therefore, the optimal firing temperature for BSAC lies between 1200 ºC and 1320 ºC.
2. The all-solid waste BSAC was successfully prepared from CA, CG, DG, and SS at a calcination temperature of 1260 ºC. It is characterized by its rapid strength development and high early strength, and it meets the SAC-52.5 standard as specified in GB 20472-2006.
3. Compared with traditional PC clinker, all-solid waste BSAC clinker has significant environmental benefits: it uses industrial solid waste 100 %, reduces energy consumption by about 18 % and carbon emissions by 65 %.

The feasibility of preparing green BSAC clinker using CA, CG DG and SS from the aspects of technology, properties, and environment were demonstrated in this work. This will help to improve the resource utilization rate of CA, CG and SS, and at the same time, reduce the consumption of natural resources and pollution to the environment by the cement industry to achieve the purpose of low-carbon production.

Acknowledgments

This research work was supported by the Science and Technology Plan Program of Inner Mongolia (Grant No. 2021GG0317, 2022YFDZ0023, 2023YFDZ0049), Scientific and technological development funds of central guidance for local (Grant No. 2022ZY0160), Basic research business funds for universities directly under Inner Mongolia Autonomous Region (Grant No. JY20230117, JY20220179), Science and Technology Plan Program of Ordos (Grant No. YF20232358) and the National Natural Science Foundation Program of China (Grant No. 52068059, 52368036).

Authorship contribution statement

Cunyong Sun: Methodology, Visualization, Formal analysis, Writing-Original draft.
Changwang Yan: Conceptualization, Writing-review & editing, Investigation, Funding acquisition.
Ju Zhang: Data curation, Writing-review & editing, Funding acquisition.
Ru Bai: Supervision, Conceptualization, Data curation.
Lei Jing: Data curation, Writing-review & editing.
Tungalagtamir Bold: Data curation, Writing-review & editing.

Declaration of competing interest

The authors of this article declare that they have no financial, professional or personal conflicts of interest that could have inappropriately influenced this work.

REFERENCES

1. Xiaoli W, Zhongcai L. 2022. Composition Design and Sintering Process of Solid Waste Based Low Calcium Carbon Fixing Cement Clinker. J Build Mater. 25(11):1115-1120. (In Chinese)
2. National Bureau of Statistics. 2024. 2023 Statistical Bulletin of the People's Republic of China on National Economic and Social Development. https://www.stats.gov.cn.
3. Gao T, Dai T, Shen L, Jiang L. 2021. Benefits of using steel slag in cement clinker production for environmental conservation and economic revenue generation. J Clean Prod. 282:124538. https://doi.org/10.1016/j.jclepro.2020.124538
4. Linag C, Xing Y, Hou X. 2024. Optimization of properties of aeolian sand cement-based materials by metakaolin. J Inner Mongolia Univ Technol (Nat Sci Ed). 43(03):278-283.
5. Sun C, Zhang J, Yan C, Yin L, Wang X, Liu S. 2022. Hydration characteristics of low carbon cementitious materials with multiple solid wastes. Constr Build Mater. 322:126366. https://doi.org/10.1016/j.conbuildmat.2022.126366

6. Su D, Yue G, Li Q, Guo Y, Gao S, Wang L. 2019. Research on the preparation and properties of high belite sulphoaluminate cement (HBSAC) based on various industrial solid wastes. Mater. 12(9):1510. https://doi.org/10.3390/ma12091510
7. Tang J, Wang Q, Zhou W, Gong X, Chen J, Huang C, Chang X. 2024. Effect of calcium sulfate type and dosage on the properties of high-belite sulfoaluminate cement. J Sustain Cement-Based Mater. 13(6):829-840. https://doi.org/10.1080/21650373.2024.2302087
8. He W, Li R, Nie D, Zhang J, Wang Y, Zhang Y, Chen Q. 2022. Belite-calcium sulphoaluminate cement prepared by EMR and BS: Hydration characteristics and microstructure evolution behavior. Constr Build Mater. 333:127415. https://doi.org/10.1016/j.conbuildmat.2022.127415
9. Hanein T, Galvez-Martos JL, Bannerman MN. 2018. Carbon footprint of calcium sulfoaluminate clinker production. J Clean Prod. 172:2278-2287. https://doi.org/10.1016/j.jclepro.2017.11.183
10. Huo G, Jiang X, Sun X, Li H, Shi H. 2024. Performance of high-belite calcium sulfoaluminate cement subjected to hydrochloric and sulfuric acid. Front Mater. 10:1282919. https://doi.org/10.3389/fmats.2023.1282919
11. Wang X, Guo MZ, Yue G, Li Q, Ling TC. 2022. Synthesis of high belite sulfoaluminate cement with high volume of mixed solid wastes. Cement Concr Res. 158:106845. https://doi.org/10.1016/j.cemconres.2022.106845
12. Yao BW, Mei SG, Luo YH, Lv CJ. 2008. Clinker Calcination and Compressive Strength of High Belite Sulphoaluminate Cement [J]. Bull Chin Ceram. 27(3):601-605. (In Chinese)
13. Hou PK, Qian JS, Wang Z, Deng C. 2012. Production of quasi-sulfoaluminate cementitious materials with electrolytic manganese residue. Cement Concr Compos. 34(2):248-254. https://doi.org/10.1016/j.cemconcomp.2011.10.003
14. Gallardo M, Almanza JM, Cortés DA, Escobedo JC, Escalante-García JI. 2014. Synthesis and mechanical properties of a calcium sulphoaluminate cement made of industrial wastes. Mater Construcc. 64(315):e023. https://doi.org/10.3989/mc.2014.04513
15. Yanze GAN, Nana A, Lemougna PN, Kaze RC, Tome S, Rahier H, Chinje FU. 2024. Development of calcium sulfoaluminate cements from rich - alumina bauxite and marble wastes: Physicochemical and microstructural characterization. Int J Ceram Eng Sci. 6(3):e10216. https://doi.org/10.1002/ces2.10216
16. Zhang J, Cui K, Yang Y, Chang J. 2024. Investigation on the preparation of low carbon cement materials from industrial solid waste phosphogypsum: Clinker preparation, cement properties, and hydration mechanism. J Clean Prod. 452:142203. https://doi.org/10.1016/j.jclepro.2024.142203
17. Tang VL, Nguyen DTL, Samchenko SV. 2019. Effect of ash-and-slag waste on the properties of sulphoaluminate portland cement. Vestnik MGSU. 14(8):991-1003. https://doi.org/10.22227/1997-0935.2019.8.991-1003
18. Gao Q, Liu L, Song X, Bai R. 2024. Enhancing strength of cement solidified Zn^{2+} and phenol contaminated soil with slag geopolymer. J Inner Mongolia Univ Technol (Nat Sci Ed). 43(01):77-81.
19. Rungchet A, Chindaprasirt P, Wansom S, Pimraksa K. 2016. Hydrothermal synthesis of calcium sulfoaluminate–belite cement from industrial waste materials. J Clean Prod. 115:273-283. https://doi.org/10.1016/j.jclepro.2015.12.068
20. Yanze GAN, Tiffo E, Nana A, Kamseu E, Chinje FU. 2024. Effects of recycled scrap alumina on the physical and mechanical properties of calcium sulfo-aluminate cement products. J Build Pathol Rehabil. 9(1):63. https://doi.org/10.1007/s41024-024-00413-7
21. Ren C, Wang W, Yao Y, Wu S, Yao X. 2020. Complementary use of industrial solid wastes to produce green materials and their role in CO_2 reduction. J Clean Prod. 252:119840. https://doi.org/10.1016/j.jclepro.2019.119840
22. You ZJ, Pan D, Shuang L D. 2012. Research on mineral formation mechanism of pulverized coal combustion boiler co-generating q-phase cement clinker. Adv Mater Res. (512-515):1687-1691. https://doi.org/10.4028/www.scientific.net/amr.512-515.1687
23. Li J, Dong W, Zhao X, Li H. 2024. Investigation on fracture properties of concrete considering the viscoelastic characteristics. Constr Build Mater. 426:136044. https://doi.org/10.1016/j.conbuildmat.2024.136044
24. Zhang S, Shuai G. 2011. Batching Calculation of Belite Sulphoaluminate Cement Clinker. J Nanchang Univ (Eng Technol). 33(1):30-32. (In Chinese)
25. Methods for chemical analysis of cement: (GB/T 176-2008) [S]. 2008. Beijing: Ministry of Housing and Urban-Rural Development of China.
26. Yuan YC. 2012. Influence of the iron phase on formation and performanceof barium calcium sulphoaluminate cement (Master's thesis, Jinan University).
27. Zhou Z. 2010. Cement Chemistry. China Light Industry Press, Inc. New York.
28. Li J. 2013. Study on high belite-sulfoaluminate cement [PhD dissertation]. Wuhan (China): Wuhan University of Technology. (In Chinese)
29. Huiling G, Junlin X. 2011. Thermodynamics and kinetics of calcium sulphoaluminate. J Wuhan Univ Technol Mater Sci Ed. 26(4):719-722. https://doi.org/10.1007/s11595-011-0300-7
30. Hajjaji M, Kacim S. 2004. Clay - calcite mixes: sintering and phase formation. Br Ceram Trans. 103(1):29-32. https://doi.org/10.1179/096797804225012701
31. Ptáček P, Opravil T, Šoukal F, Havlica J, Holešinský R. 2013. Kinetics and mechanism of formation of gehlenite, Al–Si spinel and anorthite from the mixture of kaolinite and calcite. Solid State Sci. 26:53-58. https://doi.org/10.1016/j.solidstatesciences.2013.09.014
32. Li L, Zhang Y, Zhang Y, Sun J, Hao Z. 2016. The thermal activation process of CG selected from zhungeer in China. J Therm Anal Calorim. 126(3):1559-1566. https://doi.org/10.1007/s10973-016-5711-4
33. Bullerjahn F, Schmitt D, Haha MB. 2014. Effect of raw mix design and of clinkering process on the formation and mineralogical composition of (ternesite) belite calcium sulphoaluminate ferrite clinker. Cem Concr Res. 59:87-95. https://doi.org/10.1016/j.cemconres.2014.02.004
34. Ren C. 2019. Experimental study on preparation and application of sulphoaluminate –phosphate cementitious composite material using industrial solid waste [Doctoral dissertation]. Shandong (China): Shandong University. (In Chinese)
35. Zhao G. 2004. The research of desulfurization behavior of cement raw and formulation mechanism of sulphoaluminate [Doctoral dissertation]. Wuhan (China): Wuhan University of Technology. (In Chinese)
36. Kalinkin AM, Kalinkina EV, Zalkind OA, Makarova TI. 2005. Chemical interaction of calcium oxide and calcium hydroxide with CO_2 during mechanical activation. Inorg Mater. 41(10):1073-1079. https://doi.org/10.1007/s10789-005-0263-1
37. Mutch GA, Anderson JA, Vega-Maza D. 2017. Surface and bulk carbonate formation in calcium oxide during CO_2 capture. Appl Energy. 202:365-376. https://doi.org/10.1016/j.apenergy.2017.05.130
38. Yin Y, Yin J, Zhang W, Tian H, Hu Z, Ruan M, et al. 2017. Ft-ir and micro-raman spectroscopic characterization of minerals in high-calcium coal ashes. J Energy Inst. 91(3):389–396. https://doi.org/10.1016/j.joei.2017.02.003
39. Lu W. 1989. Infrared spectroscopy of minerals. Chongqing University Press. (In Chinese)
40. Wenshi P. 1982. Collection of infrared spectra of minerals. Science Press. (In Chinese)
41. Nirmala G, Viruthagiri G. 2014. FT-IR characterization of articulated ceramic bricks with wastes from ceramic industries. Spectrochim Acta A Mol Biomol Spectrosc. 126(10):129-134. https://doi.org/10.1016/j.saa.2014.01.143

42. Perná I, Šupová M, Hanzlíček T. 2018. Gehlenite and anorthite formation from fluid fly ash. J Mol Struct. 1157:476-481. https://doi.org/10.1016/j.molstruc.2017.12.084
43. Zapata JF, Gómez M, Colorado HA. 2017. Structure-property relation and weibull analysis of calcium aluminate cement pastes. Mater Charact. 134:9-17. https://doi.org/10.1016/j.matchar.2017.10.010
44. Liu L, Zhang W, Ren X, Ye J, Zhang J, Qian J. 2021. Formation, structure, and thermal stability evolution of ternesite based on a single-stage sintering process. Cement Concr Res. 147:106519. https://doi.org/10.1016/j.cemconres.2021.106519
45. Sánchez-Herrero MJ, Fernández-Jiménez A, Palomo A. 2013. $C_4A_3\check{S}$ hydration in different alkaline media. Cement Concr Res. 46:41-49. https://doi.org/10.1016/j.cemconres.2013.01.008
46. Hughes TL, Methven CM, Jones TG, Pelham SE, Fletcher P, Hall C. 1995. Determining cement composition by Fourier transform infrared spectroscopy. Adv Cement Based Mater. 2(3):91-104. https://doi.org/10.1016/1065-7355(94)00031-8
47. Mollah MYA, Yu W, Schennach R, Cocke DL. 2000. A Fourier transform infrared spectroscopic investigation of the early hydration of Portland cement and the influence of sodium lignosulfonate. Cement Concr Res. 30(2):267-273. https://doi.org/10.1016/s0008-8846(99)00243-4
48. Winnefeld F, Lothenbach B. 2010. Hydration of calcium sulfoaluminate cements—Experimental findings and thermodynamic modelling. Cement Concr Res. 40(8):1239-1247. https://doi.org/10.1016/j.cemconres.2009.08.014
49. Jahn C, Schafföner S, Ode C, Jansen H, Aneziris CG. 2018. Investigation of calcium zirconate formation by sintering zirconium dioxide with calcium hydroxide. Ceram Int. 44(10):11274-11281. https://doi.org/10.1016/j.ceramint.2018.03.172
50. Xu B, Liu Q, Ai B, Ding S, Frost RL. 2018. Thermal decomposition of selected coal gangue. J Therm Anal Calorim. 131(2):1413-1422. https://doi.org/10.1007/s10973-017-6687-4
51. Qi YF, Dai WB, Wang Y, Gou HP, Chen XG, Pei ZY, Chen SX. 2022. Thermal decomposition properties and sulfurization reaction of gypsum. China Nonferrous Metall. (01):8-14. (In Chinese)
52. Lyu H, Hao L, Zhang S, Poon CS. 2023. High-performance belite rich eco-cement synthesized from solid wastes: Raw feed design, sintering temperature optimization, and property analysis. Resour Conserv Recycl. 199:107211. https://doi.org/10.1016/j.resconrec.2023.107211
53. Yuan BR, Nie ZR, Xiang-Hua DI, Zuo TY. 2006. Life cycle inventories of fossil fuels in China (II): final life cycle inventories. Mod Chem Ind. 26(4):59-61. (In Chinese)
54. Cui YL, Sun RJ, Zhao YN, Niu YQ. 2016. Carbon emission accounting study on entire life circle of coal-made gas [J]. Resour&Ind. 20(6):52-60. (In Chinese)
55. Ding N, Yang JX. 2015. Life cycle inventory analysis of fossil energy in China. China Environ Sci. 35(5):1592-1600.
56. Ren C, Wang W, Mao Y, Yuan X, Song Z, Sun J, Zhao X. 2017. Comparative life cycle assessment of sulfoaluminate clinker production derived from industrial solid wastes and conventional raw materials. J Clean Prod. 167:1314-1324. https://doi.org/10.1016/j.jclepro.2017.05.184
57. Wu M, Jiang GQ, Jia FR, Liu GX, Yue Q. 2018. Carbon emissions from the petroleum industry based on the analysis of material flow and life cycle[J]. Resour Sci. 40(6):1287-1296.
58. Ding N, Yang JX, Lu B. 2016. Life cycle inventory analysis of provincial thermal electricity in China. Acta Ecol Sin. 36(22):7192-7201. (In Chinese)
59. Ma L, Hong Z, Gong X. 2006. Life cycle inventory analysis of two types of freight transport on city roads. In: Beijing international materials week and China materials seminar. p. 3–8.
60. Li C, Nie Z, Cui S, Gong X, Wang Z, Meng X. 2014. The life cycle inventory study of cement manufacture in China. J Clean Prod. 72:204-211. https://doi.org/10.1016/j.jclepro.2014.02.048
61. Zhang TH, Liu B, Li JT, Hao YD, Zhang LL. 2016. The current situation and development orientation of steel slag grinding technology. Environ Eng. (S1):4. (In Chinese)
62. The norm of energy consumption per unit products of cement: GB/T 16780-2012 [S]. 2012. Beijing: Ministry of Housing and Urban-Rural Development of China.
63. Popescu CD, Muntean M, Sharp JH. 2003. Industrial trial production of low energy belite cement. Cement Concr Compos. 25(7):689-693. https://doi.org/10.1016/s0958-9465(02)00097-5
64. Khachani M, El Hamidi A, Halim M, Arsalane S. 2014. Non-isothermal kinetic and thermodynamic studies of the dehydroxylation process of synthetic calcium hydroxide. J. Mater. Environ. Sci. 5(2):615-624.
65. Tan G, Tang D, Mu T, Xu C, Wang D, Wang Q. 2014. The validity of nonlinear isoconversional method in the kinetic analysis of calcium carbonate decomposition under isothermal and non-isothermal conditions. Thermochim Acta. 585:21-24. https://doi.org/10.1016/j.tca.2014.03.041